Original Research
Vadose Zone Journal

Deterministic Analysis and Upscaling of Bromide Transport in a Heterogeneous Vadose Zone

Eran Segal, Peter Shouse, and Scott A. Bradford*

Conservative solute transport experiments were conducted at a field plot and on an undisturbed soil core from the same site. The hydraulic and solute transport properties were extensively characterized so that the data could be analyzed from a deterministic perspective. To investigate the influence of scale and conceptual model on solute transport in the relatively homogeneous upper soil profile of the field site, breakthrough curves that were collected at different depths in the undisturbed column and in the field experiments were compared and analyzed. The mobile-immobile model provided a physically realistic description of the column data that was largely independent of the transport distance, and upscaling from the undisturbed core to the field plot was relatively successful. Mean and variance of the Br^- travel times were controlled by plot-scale variability in soil water content and heterogeneity, which was overcome by averaging the concentration values from four locations at the same depth and time, and analyzing the Br^- transport behavior as a one-dimensional process. Differences between the measured and simulated mass balances, average concentration, and the variations in concentration were predicted reasonably well across depth and time. Although prediction of the exact concentration information at a given point was not achieved, this study demonstrates that area-average Br^- transport in a heterogeneous vadose zone can be deterministically quantified.

Abbreviations: BTC, breakthrough curve; CDE, convection–dispersion equation; MIM, mobile–immobile model; PSD, particle size distribution; TDR, time domain reflectometry.

A wide variety of agricultural and industrial chemicals have purposely or inadvertently been introduced into the vadose zone (Böhlke, 2002; Hamilton et al., 2007). Although many of these chemicals serve beneficial purposes, some may pose a risk to food and water supplies, as well as soil quality. For example, the presence of heavy metals and salts in the root zone can diminish soil fertility and crop yields (Mass and Hoffman, 1977; Wani et al., 2007). Furthermore, infiltrating water can leach chemicals such as nutrients (Kellogg et al., 2000), pesticides (Arias-Estévez et al., 2008), hormones (Hanselman et al., 2003), and antibiotics (Peterson et al., 2000) from the vadose zone to groundwater that serves as drinking water. Accurate knowledge of transport processes in the vadose zone is therefore needed to predict the chemical transport potential in risk assessment and in the design of remediation and management practices.

Mathematical models are commonly used to predict solute transport in the vadose zone (van Genuchten and Shouse, 1989; Jury and Roth, 1990; Bajracharya and Barry, 1997). Deterministic formulations for field-scale conservative solute transport have commonly been based on solution of the convection–dispersion equation (CDE) (Bear and Bachmat, 1967) or the mobile–immobile model (MIM) (van Genuchten and Wierenga, 1977). The conceptual model choice provides one source of uncertainty in solute transport predictions (Roth et al., 1991). Parameter values that are required by these models are typically measured in the laboratory on small-scale core samples (Hopmans et al., 2002) or are estimated from literature values. Uncertainty in model parameter values provides another source of error in predictions (Jury and Fluhler, 1992).

To validate model predictions, a limited number of field-scale solute transport experiments have been conducted in the vadose zone (Biggar and Nielsen, 1976; Jury et al., 1982; Jury and Sposito, 1985; Hills et al., 1991; Jaynes and Rice, 1993; Casey et al., 1998; Al-Jabri et al., 2002; Abbasi et al., 2003). Deviation between model predictions and field observations, however, has frequently been observed (Hills et al., 1991; Roth et al., 1991). A variety of explanations have been proposed for these observations, such as lack of information on the heterogeneous distribution of soil hydraulic and solute transport properties, spatial variability in initial and boundary conditions (Jury and Fluhler, 1992), and scale dependency of solute transport parameters (Vanderborght and Vereecken, 2007). In some cases, unstable or preferential flow has also been demonstrated to have a pronounced influence on solute transport in the vadose zone (Li and Ghodrati, 1997; Ghodrati et al., 1999; Vanderborght et al., 2000). Due to all of these complexities, a variety of solute transport model

E. Segal, Dep. of Environmental Sciences, Univ. of California, Riverside, CA; and P. Shouse and S.A. Bradford, U.S. Salinity Lab., Riverside, CA 92507.
Received 6 Dec. 2008. *Corresponding author (Scott.Bradford@ars.usda.gov).

Vadose Zone J. 8:601–610
doi:10.2136/vzj2008.0173

formulations have been developed based on stochastic methods, stream tube models, scaling approaches, and inverse simulations (Jury, 1985; Zhang et al., 2003; Zhu and Mohanty, 2002; Thomasson et al., 2006). Several reviews have recently appeared in the literature on these topics (Harter and Hopmans, 2004; Vereecken et al., 2007).

The overall objective of this study was to investigate the transport behavior of Br^- in the heterogeneous vadose zone of a field plot. To this end, transport experiments were conducted at the field plot and on an undisturbed soil core from the same site in which the hydraulic and solute transport properties were extensively characterized so that the data could be analyzed from a deterministic perspective. Our specific objectives were: (i) to validate the upscaling of transport parameters in the upper soil profile of the field site; and (ii) to demonstrate the ability to deterministically quantify Br^- transport in a heterogeneous vadose zone.

Materials and Methods

Field Experiment

The experimental field site is located in San Jacinto, CA (33°50′22″ N, 117°00′46″ W), next to a dry river bed and has a shallow perched water table at a depth of 200 cm. The experiments that are discussed here were conducted on a 6- by 6-m plot (Fig. 1). Five neutron access tubes (220 cm long) were installed vertically in the plot (Fig. 1, circle marked with Roman numerals). The water content with depth at desired times was determined using a neutron probe (503 DR Hydroprobe, CPN Int., Martinez, CA) and a calibration curve established in this soil profile.

At the corners of the plot, a backhoe was used to expose the soil profile and to install 120-cm-diameter by 220-cm-long culvert pipes vertically in the soil (Fig. 1, circles marked with letters). Each culvert pipe was instrumented with six tensiometers and six solution samplers to measure the soil water pressure and to extract the soil solution with depth. Tensiometers and solution samplers (90 cm in length) were installed horizontally from the culvert pipe into the undisturbed soil profile. The average depths of the tensiometers were 31, 61, 87, 113, 139, and 159 cm and of the solution samplers were 32, 62, 95, 126, 155, and 170 cm. The average standard deviation of the sensor depth was 6.1 cm. The solution sampler at 32 cm in the culvert pipe at Location D did not function during the experiment. A staggered configuration of the sensors in the culvert pipe was selected to minimize the potential for preferential flow and interference from other sensors and to maximize the area of the profile that was sampled (Fig. 1). The arc in Fig. 1 represents the area of water potential and soil solution sampling. Pressure transducers (MPX2100DP, Motorola Ltd., Denver, CO) and a data logger (CR7, Campbell Scientific, Logan, UT) recorded the tensiometer readings every 15 min.

To minimize the sampling time of the solution samplers, it was necessary to increase the water flux through the sampler. This was accomplished by replacing the traditional ceramic cup with filter paper (MF-0.45 mm, Millipore, Billerica, MA) that had a high saturated conductivity (60 cm h^{-1}) and a small thickness (180 μm). It should be mentioned that we decided to directly collect the soil solution in the field instead of using the time domain reflectometry (TDR) technique because accurate recovery of total Br^- using TDR is hindered by: (i) the heterogeneity of the soil profile, which induces variable water contents; and (ii) the background salinity of irrigated mineral soils (Vogeler et al., 2001). The solute travel time and center of mass measured by TDR (Kachanoski et al., 1992) therefore provides only limited information on solute transport under heterogeneous field conditions.

A detailed description of soil stratigraphy, hydraulic properties, and water flow patterns at the field plot was given by Segal et al. (2008). Only an abbreviated discussion is given below. The soil cores from the neutron access tube installation at the field site (Fig. 1) were collected and cut into 15-cm intervals for particle size distribution (PSD) analysis. Figure 2A presents a plot of the median grain size (d_{50}) as a function of depth for Locations I, II, and V. The upper 0- to 70-cm depth consisted of a uniform sandy loam layer that had d_{50} values of approximately 50 μm and low variability. A sandy layer occurred between 70 and 80 cm that had d_{50} values from 140 to 250 μm. Below a depth of 80 cm, the soil profile consisted of loam with sandy and silty clay loam lenses. Although the fine-textured lenses and sand layers were not visible in each profile due to the sampling method (averaging of 15 cm), variability in d_{50} values indicated their existence and the location of these layers. For example, lower d_{50} values were measured in the profile at Location II directly below the sandy layer at 90 and 175 cm, indicating the existence of fine-textured lenses. High d_{50} values, associated with sand layers, were measured in the profiles at Locations I and X at 125 and 175 cm, respectively.

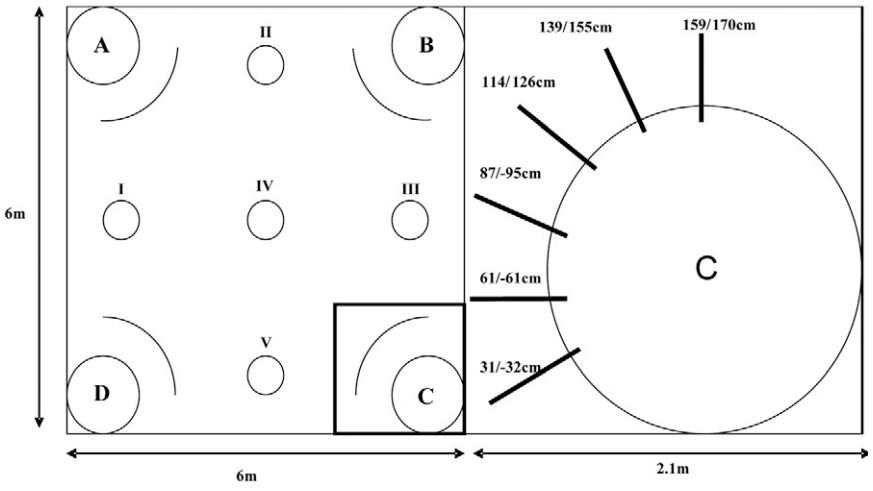

FIG. 1. A schematic illustration of the field site. The left square represents a 6- by 6-m plot. Circles with letters are 220-cm-long, vertical culvert pipes installed with six tensiometers and six soil solution samplers. Circles with roman numerals are vertical neutron probe access tubes and the arcs represent the area of sampling. The right-hand side is an enlargement of the instrumentation in the culvert pipes. The actual average installation depth of the tensiometers and solution samplers is provided.

For measurements of bulk density (ρ_b) and hydraulic properties, undisturbed soil cores were collected vertically from locations on the boundaries of the plot next to the neutron access tubes (I, II, and V in Fig. 1), with samples taken every 30 cm from the soil surface to a depth of 150 cm. Average soil ρ_b values are presented

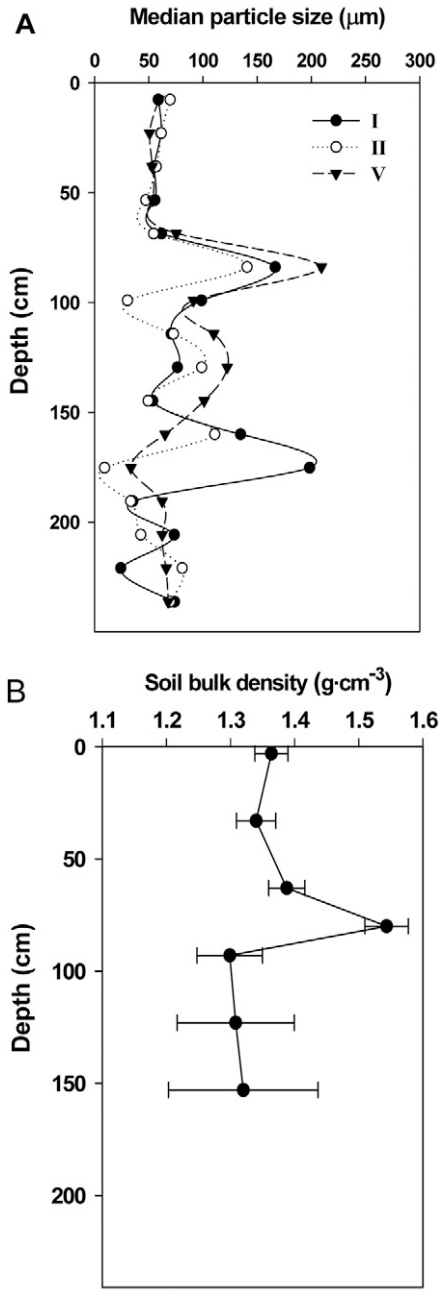

FIG. 2. (A) Median size of soil particles in 15-cm intervals from Locations I, II, and V, and (B) the soil bulk density measured at three locations. The horizontal bars are standard deviations.

in Fig. 2b; the horizontal bars provide the standard deviations. Consistent with the PSD information presented in Fig. 2A, the ρ_b values from the upper sandy loam layer (0–70 cm) were around 1.35 g cm^{-3} and exhibited low variability, the sandy layer (70–80 cm) had a high ρ_b of 1.55 g cm^{-3}, and the ρ_b values from the lower profile (>80 cm) were around 1.3 g cm^{-3} and had high variability due to the presence of sandy and silty clay loam lenses in the loam. Retention curves and the saturated hydraulic conductivity (K_s) were measured on undisturbed cores that were taken from two locations on the boundaries of the plot next to the neutron access tubes at Locations II and V and six depths (30, 60, 75, 90, 120, and 150 cm).

A steady-state conservative tracer (KBr) experiment was conducted on the plot. The tracer experiment was conducted on a bare soil, after plowing the upper 20 cm of the soil. The water application method has been found to have an effect on solute transport parameters (Jaynes and Rice, 1993). We used a 0.2- by 0.2-m staggered grid, drip irrigation system (Typhoon 630, Netafim, Fresno, CA) to uniformly apply small water and solute fluxes to the soil surface that induced unsaturated flow conditions in the upper 120 cm of the soil profile. The surface boundary condition was a steady infiltration rate of 0.275 ± 0.025 cm h^{-1}. The soil surface was covered with a black nylon tarp to avoid water evaporation during the tracer experiment. The value of the soil water pressure head, h (m), with depth was continuously monitored using tensiometers in the culvert pipes, and the water content, θ, distribution in the profile was measured using a neutron probe throughout the tracer experiments.

When a steady-state water flow condition was established in the soil profile after 100 h, the water application system was switched from well water to the KBr solution for 47 h and then switched back to well water for an additional 280 h. The KBr solution had 2.4 g L^{-1} Br^-, and was mixed well before and during application. Soil solution samples were collected during an interval of 24 h and analyzed for Br^- concentration with a calorimetric system (Flow Solution IV, O.I. Analytical, College Station, TX). The Br^- data from the field are presented at the median time of the sampling interval. Following completion of the Br^- transport experiment, the water content and pressure head in the soil profile was monitored during drainage for an extra 14 d so that the soil hydraulic properties of the root zone could be determined according to the instantaneous profile method (Watson, 1966).

Additional information was collected to evaluate the transverse dispersivity (λ_T) in the root zone (0–60 cm) and the effect of a nonuniform upper boundary condition on the soil water and Br^- application uniformity. An experiment at the boundary of the plot (next to the neutron access tube at Location I) was conducted with four emitters in a 40-cm staggered grid. A constant water flux of 0.55 cm h^{-1} for 48 h was applied to achieve a steady-state flow condition in the upper 30 cm of the soil profile, which was verified with stable water content measurements (TDR 100, Campbell Scientific, Logan, UT) with time at the center of the grid. Subsequently, the well water was switched to a KBr solution (2.4 g L^{-1} of Br^-) that was mixed well before and during application. Soil cores were sampled and analyzed for water content and Br^- as a function of distance from each emitter at a specific depth (30 cm) and time (24 h after the Br^- pulse had been initiated). Twenty soil cores, 2.5 cm long (1.25 cm in diameter), were collected at 0, 5, 10, 15, and 20 cm from the four emitters. The transverse dispersivity of the root zone was estimated by fitting simulation results to experimental data (Table 1) using the nonlinear least squares optimization routine in HYDRUS-2D.

Laboratory Experiment

An undisturbed core was taken from the field site to study the transport of KBr in the laboratory. The core was sampled just outside of the field plot adjacent to the neutron access tube at Location V (Fig. 1). The core length was 65 cm and the internal diameter was 24 cm. An acrylic cylinder with a sharp edge at the bottom was pushed into the soil with a hydraulic piston. The core was dug out and brought to the lab in a polyvinyl chloride sleeve with caps on both ends. The core was subsequently situated in a temperature-controlled laboratory with a ceramic

TABLE 1. Measured and simulated volumetric water content and relative Br^- concentration as a function of horizontal distance from the emitter at depth of 30 cm.

Horizontal distance from the emitter	Volumetric water content		Relative Br^- concentration (C/C_0)	
	Measured	Simulated	Measured	Simulated
cm	$m^3\ m^{-3}$			
0	0.35 ± 0.03	0.37	1.00 ± 0.13	1
5	0.36 ± 0.02	0.37	0.95 ± 0.12	0.98
10	0.36 ± 0.01	0.37	0.90 ± 0.03	0.93
15	0.36 ± 0.005	0.37	0.80 ± 0.08	0.80
20	0.35 ± 0.01	0.37	0.67 ± 0.16	0.67

plate (bubbling pressure of 100 kPa) at the bottom (Soilmoisture Equipment Corp., Santa Barbara, CA). Two tensiometers (Soilmoisture Equipment Corp.) connected to pressure transducers (143PC05D, Honeywell, Morristown,NJ) were installed at 15 and 45 cm from the soil surface to monitor the matric potential throughout the experiment.

In contrast to the field study, TDR probes were preferred over direct solution sampling in the one-dimensional column study because of the relatively uniform soil profile in the upper 65 cm and the ability to recover all of the Br^- in the effluent. Two TDR probes (three rods of 20-cm length and 3.175-mm diameter), connected to a TDR100 (Campbell Scientific, Logan, UT), were installed at 30- and 52.5-cm depths to monitor the water content and the soil apparent electrical conductivity (EC_a) throughout the experiment (Ward et al., 1994). A CR10X datalogger (Campbell Scientific) was used for data acquisition at 15-min intervals during the tracer experiment. The soil solution was also sampled at the column output (65 cm) with time (in 1-h intervals) and analyzed for electrical conductivity (EC). The column was located on a balance (CD-11, Ohaus, Pinebrook, NJ) so that the total mass of the column throughout the experiment could be monitored to ensure steady-state water flow.

The soil surface boundary condition during the tracer experiment was a steady-state infiltration rate of 0.396 cm h^{-1} that was applied uniformly to the column surface using a high-performance liquid chromatography pump (Series II, LabAlliance, State College, PA) and a plastic pouch with membrane wall (Sisson and Shouse, personal communication, 2007). The lower boundary condition was adjusted by using the hanging water column method and set to be h = –32.5 cm. This value matched the measured h at this depth in the field plot during the tracer experiment. After a steady-state flow condition was established with well water from the field site (verified with tensiometer, TDR, and balance readings), KBr solution was applied for 47 h and switched back to well water for an additional 200 h. The KBr solution consisted of 2.4 g L^{-1} of Br^- (EC of 4.5 dS m^{-1}) that was continuously mixed during application. Bromide concentrations were correlated to the EC_a values (Ward et al., 1994) that were measured with the TDR probes or the solution EC of the effluent measured with an EC meter (M33.1, Agricultural Electronics, Montclair, CA). The background EC_a in the soil based on the TDR readings, background EC in the effluents, and Br^- mass balance was used to determine the maximum concentration of Br^- at each depth.

A drainage experiment was also conducted on the soil core to investigate the similarity of the core and the field hydraulic properties at the plot. The drainage experiment was initiated by connecting the bottom outlet of the core to a reservoir filled with well water, which was lifted to achieve zero pressure head at the soil surface and to saturate the core. The soil surface was covered with a nylon tarp to avoid evaporation. After the soil core was saturated, the water table was dropped 35 cm below the ceramic plate. Pressure heads, water contents, and weight were subsequently recorded for 33 h during the drainage process.

Simulations

HYDRUS-1D (Šimůnek et al., 1998) was used to simulate the drainage and transport of Br^- in the undisturbed core. In addition, it was used to simulate the transport of Br^- in the root zone of the field plot. The governing equation for water flow that was solved is (Richards, 1931)

$$\frac{\partial \theta}{\partial t} = \frac{\partial}{\partial z}\left[K(h)\frac{\partial h}{\partial z}\right] + \frac{\partial K(h)}{\partial z} \qquad [1]$$

where θ is the volumetric water content ($m^3\ m^{-3}$), h is the soil water pressure head (cm), K is the hydraulic conductivity (cm h^{-1}), t is time (h), and z is the distance in the vertical direction (cm). The van Genuchten–Mualem hydraulic model (van Genuchten, 1980) was used:

$$\begin{aligned} \mathrm{Se} &= \frac{\theta - \theta_r}{\theta_s - \theta_r} \\ \mathrm{Se}(h) &= 1 \qquad h \geq 0 \\ \mathrm{Se}(h) &= \frac{1}{\left(1 + |\alpha_{VG} h|^{n_{VG}}\right)^{m_{VG}}} \qquad h < 0 \end{aligned} \qquad [2]$$

where

$$m_{VG} = 1 - \frac{1}{n_{VG}}$$

$$K(\mathrm{Se}) = K_s \mathrm{Se}^{0.5}\left[1 - \left(1 - \mathrm{Se}^{1/m_{VG}}\right)^{m_{VG}}\right]^2$$

where θ_s and θ_r are the saturated and residual volumetric water contents ($m^3\ m^{-3}$), respectively, K_s is the saturated hydraulic conductivity (cm h^{-1}), and α_{VG} (cm^{-1}), n_{VG}, and m_{VG} are soil-specific water retention curve parameters. Solute transport was quantified using the MIM equations (van Genuchten and Wierenga, 1977):

$$\frac{\partial \theta_m c_m}{\partial t} + \theta_{im}\frac{\partial c_{im}}{\partial t} = D_L \frac{\partial^2 \theta_m c_m}{\partial z^2} - \frac{\partial v_m \theta_m c_m}{\partial z} \qquad [3]$$

where

$$\theta_{im}\frac{\partial c_{im}}{\partial t} = \alpha(c_m - c_{im})$$

v is the average pore water velocity (cm h^{-1}), D_L is the diffusion–dispersion coefficient ($cm^2\ h^{-1}$), α is the first-order mass transfer coefficient (h^{-1}), and c is the resident solute concentration (g L^{-1}). The superscripts m and im are used to denote variables that are associated with the mobile and immobile fractions of the soil space, respectively. The solute dispersivity (λ_{MIM}) is equal to D_L/v_m. The CDE model can be derived from Eq [3] by setting the immobile water content (θ_{im}) to zero.

The drainage process in the undisturbed core was simulated using HYDRUS-1D to obtain an independent estimate of the hydraulic properties. The total simulation domain was 66 cm in length, with the upper 65 cm consisting of a sandy loam soil and the bottom 1 cm representing the ceramic plate. The porosity and saturated hydraulic conductivity of the 1-bar ceramic plate was 0.45 and 0.031 cm h^{-1}. The column was initially saturated, and the value of h was therefore linearly distributed from 0 at the top of the column to 66 cm at the bottom of the column. The upper boundary condition during the drainage simulation was zero flux and the bottom boundary condition was a constant pressure head of −35 cm. A total of 33 h of water drainage was simulated under these boundary conditions. The parameter values of the hydraulic property model were obtained by fitting the simulation results to the measured data using a nonlinear optimization routine in the model. The fitted hydraulic properties for the undisturbed soil core are given in Table 2.

Bromide transport through the undisturbed soil core and the root zone of the field plot were also simulated using HYDRUS-1D. Initially, the soil profiles were assumed to have zero Br^- and to be under hydrostatic conditions. The upper boundary for water flow was a constant flux of 0.396 cm h^{-1} in the undisturbed core and 0.275 cm h^{-1} in the field. After 50 h of simulated water flow, the Br^- tracer solution (2.4 g L^{-1}) was added for a specific pulse duration (47 h) using a third-type boundary condition and then flushed with water for an additional 200 h. The lower boundary (z = 65 cm in the core and z = 60 cm in the field) was similar to the field-measured h at this depth and modeled as a constant-head boundary condition (h = −32.5 cm in the core and h = −35 cm in the field). The solute transport parameters λ_{MIM}, θ_{im}, and α were estimated by fitting experimental data from the core to simulated data using the nonlinear least squares optimization routine in HYDRUS-1D.

The HYDRUS-2D code (Šimůnek et al., 1999) was used to simulate the two-dimensional water flow and Br^- transport at the field site during the tracer experiment under a nonuniform upper boundary condition (drip) and when considering a heterogeneous distribution of hydraulic properties in the lower profile (depths >80 cm). In this case, equations analogous to Eq. [1] and [3] were used, but for two spatial dimensions. Based on the plot size and the profile depth, the simulation domain was selected to be 200 cm in the vertical direction and 500 cm the horizontal direction. The simulated profile was consistent with the stratigraphy that was determined from the PSD and bulk density information (Fig. 2). In particular, the simulation considered a sandy loam layer from a depth of 0 to 60 cm, a sand layer from a depth of 70 to 80 cm, and a heterogeneous loam layer from 80 to 175 cm that contained lenses of sand and silty clay loam. Segal et al. (2008) provided a complete description of how the heterogeneous distribution of hydraulic properties in the lower profile were generated from measured PSD and ρ_b information, hydraulic properties measured on core samples, pedotransfer functions, and interpolation algorithms. Table 2 provides values of the measured hydraulic properties for these simulations. The MIM transport parameters for each soil layer and lens were based on the findings of the current study (depths of 0–70 cm) or were estimated from literature values (Casey et al., 1998; Zurmuhl, 1998; Al-Jabri et al., 2002; Abbasi et al., 2003). The transverse dispersivity of other textures was assumed to be 50% of the measured literature values of the longitudinal dispersivity (λ_L).

For the HYDRUS-2D simulations, the field soil profile was initially assumed to have zero Br^- and to be under hydrostatic conditions. A nonuniform water application at the upper boundary was simulated using a drip-line source with 20-cm spacing. The upper boundary for water flow was a constant flux of 0.275 cm h^{-1}. After 96 h of simulated water flow, the Br^- tracer solution (2.4 g L^{-1}) was added for a specific pulse duration (47 h) using a third-type boundary condition and then flushed with water for an additional 300 h. The lower boundary (200-cm depth) was set to a constant water pressure head of 50 cm, where a local rise in the water table was observed and no flow was set on the sides of the model domain. The average Br^- concentrations for each depth at selected times were subsequently calculated.

Results and Discussion

Laboratory Experiment

The drainage process in the undisturbed core was simulated to determine the soil hydraulic properties. The fitted hydraulic properties of the soil in the column are given in Table 2. These values compare favorably with values of the hydraulic properties that were previously measured in the field at this site (Table 2), suggesting that the undisturbed core provided a reasonable approximation of water behavior under field conditions.

A Br^- transport experiment was conducted on the undisturbed core that was taken from the field plot to minimize any technical problems that existed in the field studies (i.e., low water application uniformity, long sampling interval, full recovery of the effluent, and temperature variation) and to study the influence of scale on Br^- transport. Figure 3 presents measured and simulated relative concentrations for Br^- in

Table 2. Hydraulic properties and transport parameters of undisturbed small cores from two locations at several depths in the field, and for a large undisturbed core.

	Field plot						Undisturbed core (0–65 cm)
Parameter†	30 cm	60 cm	70–80	90–175			
Texture	sandy loam	sandy loam	sand	loam	silty-clay loam lens	sand lens	sandy loam
θ_s, m^3 m^{-3}	0.43	0.43	0.33	0.42	0.48	0.34	0.39
θ_r m^3 m^{-3}	0.03	0.03	0.01	0.04	0.06	0.01	0.03
α_{VG}, cm^{-1}	0.012	0.012	0.016	0.007	0.0056	0.015	0.009
n_{VG}	1.63	1.59	1.96	1.57	1.72	1.89	1.58 ± 0.06
K_s, cm h^{-1}	1.8 ± 0.6	2.9 ± 0.08	71.2 ± 0.2	0.7 ± 0.27	0.45 ± 0.05	32.3 ± 0.09	2.08 ± 0.06
λ_L, cm	0.561	0.561	0.042‡	0.4‡	0.4‡	0.042‡	0.561
λ_T, cm	0.55	0.55	0.021‡	0.2‡	0.2‡	0.021‡	—
θ_{im}, m^3 m^{-3}	0.0978	0.0978	0.10‡	0.025‡	0.025‡	0.10‡	0.0978
α, h^{-1}	0.00351	0.00351	0.06‡	0.015‡	0.015‡	0.06‡	0.00351

† θ_s and θ_r, saturated and residual volumetric water contents, respectively; α_{VG} and n_{VG}, soil-specific water retention curve parameters; K_s, saturated hydraulic conductivity; λ_L and λ_T, longitudinal and transverse dispersivities, respectively; θ_{im}, immobile water content; α, first-order mass transfer coefficient.

‡ Literature value.

the undisturbed core at three depths (30, 52.5, and 65 cm) as a function of time. In this case, the breakthrough curves were simulated using the CDE and MIM models. The model parameters (λ_{CDE} or λ_{MIM}, θ_{im}, and α), their 95% confidence intervals and the coefficient of determination, R^2, are also presented in Fig. 3. The breakthrough curves simulated by the MIM model captured the observed dual slopes at the ascending section and the concentration "tailing" at later times. These findings yielded higher R^2 values than the simulated curves of the CDE model. The fitted parameters are consistent with the published literature under comparable experimental conditions (Poulsen et al., 2006; Al-Jabri et al., 2002; Casey et al., 1998).

Selection of a proper conceptual model to analyze the solute transport data minimized the uncertainty in the field-scale model predictions. Vanderborght and Vereecken (2007) and a few earlier studies (Butters and Jury, 1989; Wierenga and van Genuchten, 1989) found that flow distance has an effect on the dispersion coefficient determined using the traditional CDE (Eq. [3] with $\theta_{im} = 0$). To study the influence of the conceptual model on scale-dependent solute transport parameters, we analyzed the solute transport data from the undisturbed core (shown in Fig. 3) for each depth using the CDE model. The dispersivity of the CDE model (λ_{CDE}) increased with depth from λ_{CDE}(30 cm) = 1.432 ± 0.015 cm to λ_{CDE}(65 cm) = 1.674 ± 0.024 cm. Although this difference is small, if we use the fitted MIM model parameters to predict the solute breakthrough at a distance of 300 cm and then fit λ_{CDE} to these data, the value of λ_{CDE} will increase by an order of magnitude to 11.98 ± 0.017 cm. Our findings show that the MIM model provided a more physically realistic representation of solute transport in the undisturbed soil column, and the MIM model was therefore used to analyze the field-scale transport data.

Field Experiment

Water Flow

Measured and simulated water content and water pressure head as a function of depth at the field plot during the tracer experiment are presented in Fig. 4A and 4B. The pressure head (tensiometers in four culvert pipes) and water content (five neutron access tubes) data are average values at a given depth, and the error represents one standard deviation. High water contents and a positive pressure head value were measured below 150 cm due to the rise of the perched water table during steady-state flow. Starting at around 150-cm depth, the pressure head gradually decreased toward the soil surface. The value of θ with depth depends on both the pressure head (directly related) and the soil texture. Due to the presence of sand layers, lower values of θ occurred at approximately 90 and 180 cm. The measured water status in the undisturbed column during steady-state water flow is also illustrated in Fig. 4. The consistent values between field and column data indicate similar water flow patterns in these systems.

The water content at a depth of 30 cm as a function of horizontal distance from the drip emitter is presented in Table 1, along with measured standard deviations. These data revealed only minor changes in the horizontal distribution of water content, suggesting that the water distribution in the soil profile was not significantly affected by the drip irrigation system.

Bromide Travel Times

The transport of Br^- at the field plot is presented in Fig. 5. This figure shows measured breakthrough curves (BTCs) for Br^- at five depths (32, 61, 95, 126, 155, and 170 cm) and at four locations (the culvert pipes at Locations A, B, C, and D). The Br^- BTCs from 170 cm were not analyzed due to only partial recovery of the BTCs. In general, the BTCs at a given depth from the four locations were more similar in the root zone (32 and 61 cm) than in the lower profile (95–155 cm). Discrepancies in the shape and timing of the BTCs at a given depth from the four locations are due to several factors, namely soil heterogeneity, water content, and the location of the solution samplers.

The means and standard deviations of the Br^- travel times for each BTC are presented in Table 3, as well as the average and variance of these values at each depth. Minor changes in the variance of the mean travel time were measured in the upper profile (32 and 61 cm) due to high uniformity in soil texture (Fig. 2) and water content (Fig. 4). In contrast, the variance significantly increased immediately below the sand layer (95 cm). This high variability in travel time can be attributed to three reasons, namely: (i) the sand layer was associated with a lower water content (Fig. 4) and consequently a higher pore

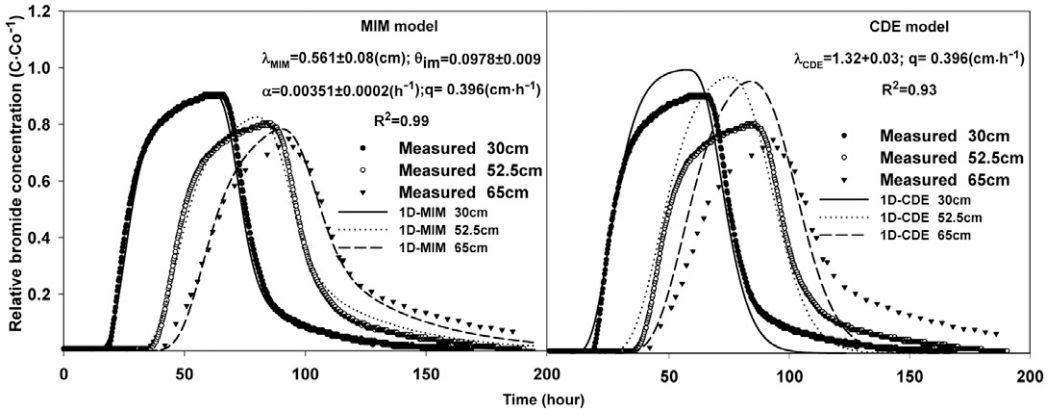

FIG. 3. Measured (symbols) and modeled (lines) relative Br^- concentration with time in an undisturbed soil core. Data are depicted for three depths: 30, 52.5, and 65 cm. The surface water flux (q) and the parameters of the (A) mobile–immobile model (MIM) and (B) convection–dispersion equation (CDE) models and their 95% confidence intervals (solute dispersivity [λ_{MIM} and λ_{CDE}], immobile water content [θ_{im}], and the first-order mass transfer coefficient [α]).

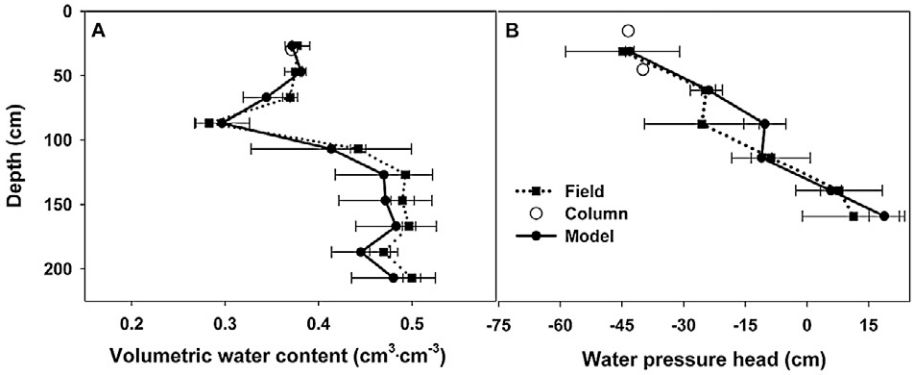

FIG. 4. Measured and simulated (A) water content and (B) water pressure head as a function of depth during steady-state infiltration in the field soil profile and the undisturbed soil core. Field data are average values from the culvert pipes at Locations A, B, C, and D and simulated data are presented as average values at these same depths. The horizontal bars are standard deviations.

water velocity; (ii) low permeability lenses just below the sand layer caused lateral flow of Br^-; and (iii) variability in the soil permeability directly below the sand layer generated variability in water and Br^- mass inputs.

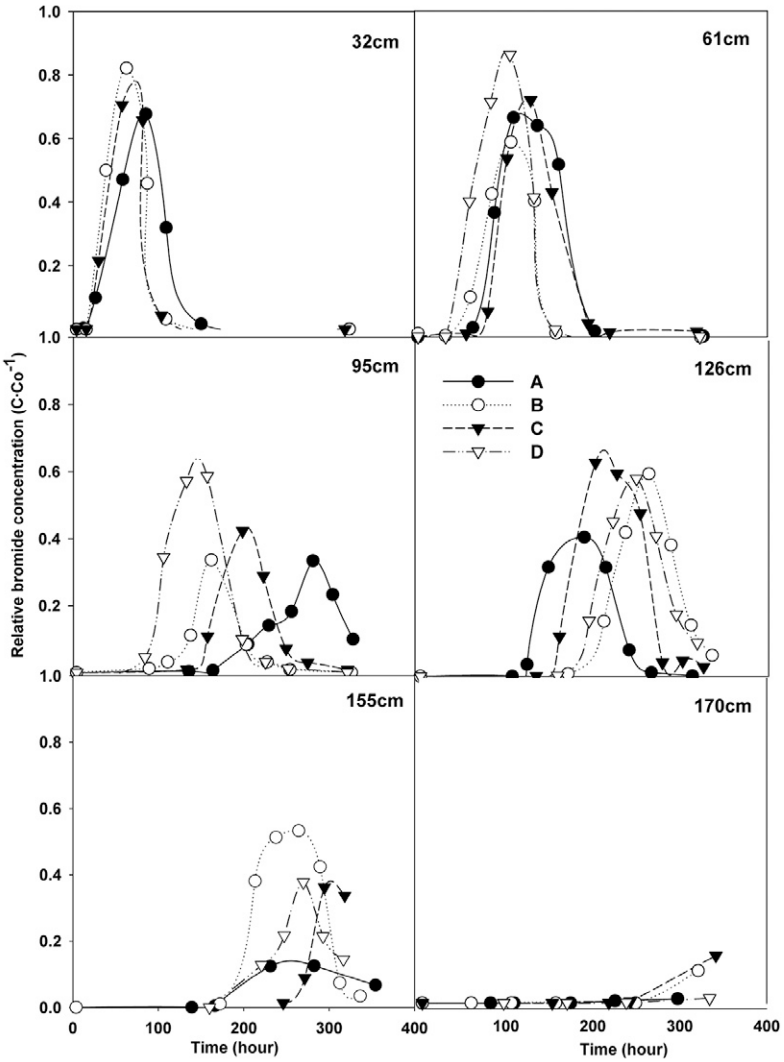

FIG. 5. Field measurements of the relative Br^- concentration with time for the Br^- tracer experiment. Data are presented at six depths in the field plot, 32, 61, 95, 126, 155, and 170 cm at four locations (A, B, C, and D).

An example of delayed Br arrival and bypassing is observed in the BTCs from the culvert pipe at Location A at depths of 95 and 126 cm (Fig. 5, Table 3). In this case, the mean travel time was 280 h at 95 cm, compared with 190 h at 126 cm. Furthermore, highly variable Br^- mass input at 95 cm is demonstrated by the significant differences in Br^- recovery from the BTCs (43–89%).

Additional evidence of the complicated Br^- transport pattern below the sand layer is the discrepancy between the average water and Br^- velocities at 95 cm. The mean pore water velocity was 0.98 cm h^{-1} (based on the average water content), whereas the mean Br^- velocity was calculated to be 0.43 cm h^{-1} (based on average Br^- travel time and distance). This difference implies that changes in the average water content with depth cannot exclusively explain the difference in the Br^- travel times. In contrast, at depths greater than 126 and 155 cm, the variance in the mean Br^- travel time decreased with depth. This observation is consistent with a decrease in pore water velocity with increasing water content (Fig. 4).

The average standard deviation in travel time (Table 3) tended to increase with depth, as expected due to dispersion. Similar values occurred at 95 and 126 cm, however, probably due to greater variability in travel times at 95 cm. The ratio between the variance and the average value was much larger for the mean travel times than the standard deviations of the travel times. This observation suggests that local-scale effects on the BTCs were much less significant than plot-scale factors.

Averaging of Bromide Transport

The influence of soil heterogeneity, water content, and the location of the solution samplers on the tracer data may be overcome by averaging the four collected samples at the same depth and time, and then analyzing the depth-averaged Br^- transport behavior. Bromide transport in the root zone and in the lower profile are discussed separately in detail below due to the differences in soil and water flow characteristics in these regions noted above.

The observed field measurements of the depth-averaged Br^- transport data are presented in Fig. 6. The

TABLE 3. Mean and standard deviation (in parentheses) of Br^- travel time at each sampling depth and culvert pipe location, and associated average and variance values for each depth.

Location	Estimated Br^- travel time				
	32 cm	61 cm	95 cm	126 cm	155 cm
	h				
A	82 (52)	120 (50)	280 (69)	190 (60)	250 (80)
B	64 (37)	110 (46)	160 (61)	265 (62)	250 (63)
C	75 (38)	130 (56)	200 (66)	210 (68)	300 (79)
D	NA†	110 (46)	145 (62)	250 (66)	270 (76)
Avg.	73.6 (42)	117.5 (50)	196.2 (65)	228.7 (64)	267.5 (75)
Variance, h^2	82.3 (70)	91.6 (22)	3656.2 (13)	1206.2 (13)	558.3 (62)

† NA, not available.

average relative Br^- concentration at a given time is denoted using filled circles for the 32-cm depth and empty circles for the 61-cm depth. Integration of the area under the BTC provided very good mass balance at 32 and 61 cm (99.5–102%), which is presented in the figure. The vertical bars represent standard deviations and the horizontal bars represent the sampling time range (24 h). Standard deviations account for the inherent soil spatial variability and the variable location of each solution sampler. The modeled BTCs, base on the MIM transport parameters evaluated in the laboratory, are also depicted in Fig. 6. The modeled curves provide a reasonable prediction of the average measured value of Br^- at 32 and 61 cm and total Br recovery. In general, the attempt to independently predict the Br^- transport in the root zone by using only laboratory-derived model parameters was fairly successful at this scale. In addition, both one- and two-dimensional simulations (average value of a cross-section at a specific depth and time) provided nearly an identical description of the data, indicating that the water flow and solute transport in the upper 60 cm of the soil profile could be described as a uniform, one-dimensional process when using our drip irrigation setup and measured values of dispersivity.

The water flow and solute transport pattern in the lower profile (70–200 cm) is much more complex than in the root zone (0–70 cm). In particular, the coarse sand layer at about 70 cm generates high water velocities and a lateral component to water flow (Segal et al., 2008). The presence of interconnected layers and fine-textured lenses of variable thickness below 80 cm produces a location-specific pattern of solute transport through the lower soil profile of the field plot. Two-dimensional solute transport simulations were conducted to study the relative importance of nonuniform boundary conditions and soil heterogeneity on solute transport in the lower profile. Results indicate that soil heterogeneity is the major contributor to solute transport behavior in the lower soil profile. Specifically, variations in Br^- travel time and total mass suggested that the sand layer in conjunction with fine-textured lenses slows down the Br^- propagation and generates bypassing of water and solute through lower resistance pathways. Yet, the lower water velocities below this region (due to the raised water table) decrease the variability in the mean travel time (Table 3) and generate a more uniform Br^- front. This finding coupled with the fact that the exact soil type that is associated with a particular soil solution sampler is unknown, hampers the application of a completely deterministic approach for describing solute transport in the lower profile.

Considering the above information, the Br^- transport data in the lower profile is presented in terms of the one-dimensional

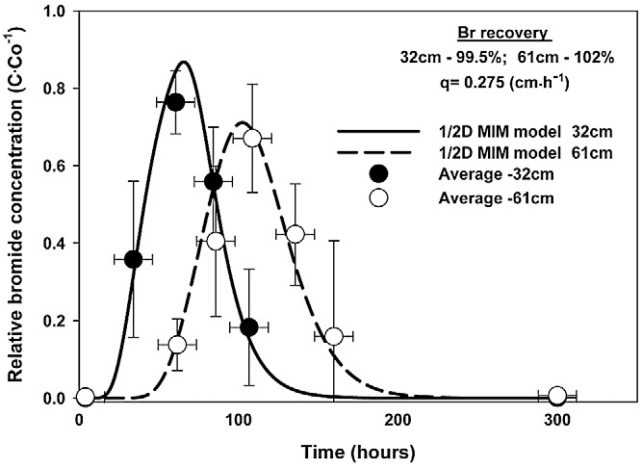

FIG. 6. Field measurements of the relative Br^- concentration with time for the Br^- tracer experiment. Data are presented at two depths in the field plot, 32 and 61 cm (circles). Each data point is an average of the four locations at the same time and depth. The vertical bars are standard deviations and the horizontal bars represent the sampling time range (24 h). The corresponding one- and two-dimensional (depth-averaged) mobile–immobile model (MIM) simulation results are also presented based on transport parameters derived from the undisturbed core.

average concentration (four sample locations) at a specific depth as a function of time. Figure 7 presents measured and simulated Br^- BTCs in the lower profile at 95, 126, and 155 cm and the Br^- mass recovery under the BTCs. The horizontal bars are standard deviations of the concentration measurements. It should be mentioned that the one-dimensional modeling data that are presented in this figure were generated from a two-dimensional simulation that was averaged across a specific depth at a given time. A transect of spatially heterogeneous hydraulic properties was generated from measurements taken from the field plot that was used as input for this simulation (Segal et al., 2008). Good agreement between measured and modeled data was found (correlation coefficient >84%). In general, travel time and the mass balance of the average Br^- concentration with depth were conserved (>88.4% Br^- mass recovery). The observed and simulated standard deviations have the same order of magnitude as the average value, however, suggesting high variability of Br^- at a specific depth and time.

Summary and Conclusions

Conservative solute (Br^-) transport experiments were conducted at a field site and on an undisturbed soil core in which the hydraulic and solute transport properties were extensively characterized so that the data could be analyzed from a deterministic perspective. The MIM provided a physically realistic description of the column data that was largely independent of the transport distance. In contrast, analysis of these same data using the CDE model indicated that the dispersivity needed to increase with transport distance. Hence, CDE predictions produced increasing errors at longer transport distances. Upscaling of MIM transport parameters from the undisturbed core to the relatively homogeneous root zone of a field plot was successful at the considered scale (<70 cm).

Analysis of the means and variances of Br^- travel times indicated that the BTC characteristics were controlled by the soil water

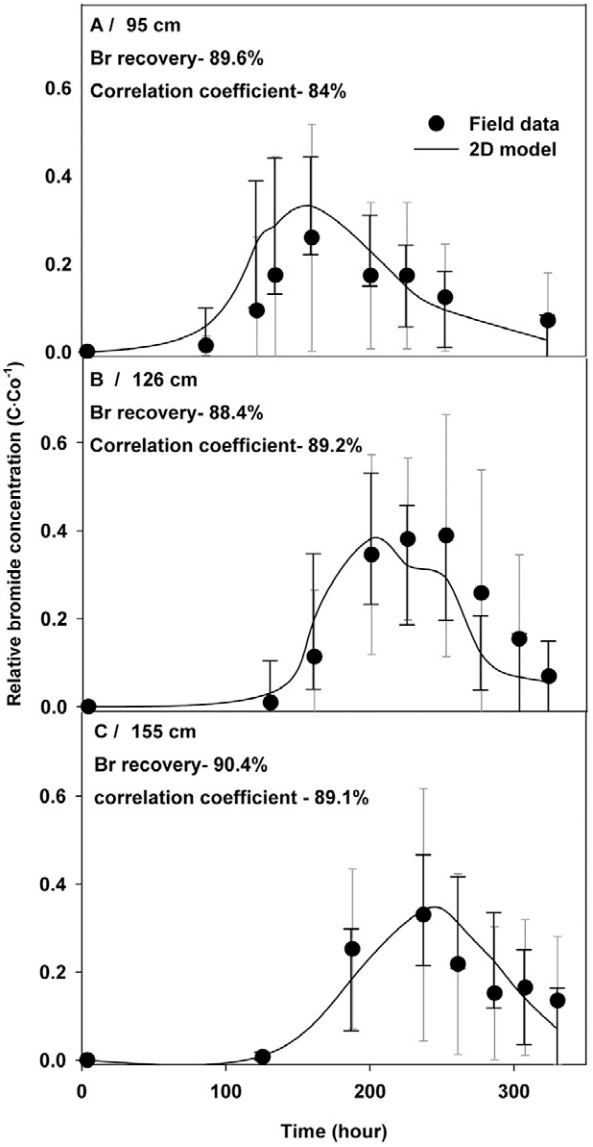

FIG. 7. Field measurements (circles) and two-dimensional mobile–immobile model simulation (lines) of relative Br^- concentrations with time at (A) 95, (B) 126, and (C) 155 cm. Measured data are average values from four sampling locations at the same time and depth. Simulated data are presented as average values at these same depths. The horizontal bars are standard deviations.

content, soil heterogeneity, and soil solution sampler location at the plot scale. Detailed information on the soil heterogeneity in the lower profile allowed physically realistic simulation of water flow and solute transport in this region. Owing to the spatial heterogeneity of soil hydraulic and transport properties and the solution sampler's location in the soil profile, field measurements and simulation results were converted to a one-dimensional form by average with depth. The averaging process utilized concentration values from four locations that were collected at the same depth and time. In this case, comparison between the measured and simulated mass balance, average concentration, and the variations in concentration were predicted reasonably well with depth and time. Although prediction of the exact concentration information at a given point was not achieved, this study demonstrates that area-average Br^- transport in a heterogeneous vadose zone can be deterministically quantified.

ACKNOWLEDGMENTS

This research was supported by the 206 Manure and Byproduct Utilization Project of the USDA-ARS and an interagency agreement with the USEPA (IAG no. DW-12-92189901-0). Although this work has been supported by the USDA and the USEPA, it has not been subjected to agency review and does not necessarily reflect the views of the agency, and no official endorsement should be inferred. Similarly, mention of trade names and company names in this manuscript does not imply any endorsement or preferential treatment by the USDA or USEPA. We would also like to acknowledge the efforts of Devin Rippner, Mai Lingh Nguyen, Jack Jobes, JoAn Fargerland, Dr. Saeed Torkzaban, and Alan Nguyen in helping to conduct the studies outlined here. We would also like to acknowledge the essential collaboration of Bruce Scott on this project.

References

Abbasi, F., J. Šimůnek, J. Feyen, M.Th. van Genuchten, and P.J. Shouse. 2003. Simultaneous inverse estimation of soil hydraulic and solute transport parameters from transient field experiments: Homogeneous soil. Trans. ASAE 46:1085–1095.

Al-Jabri, S.A., R. Horton, D.B. Jaynes, and A. Gaur. 2002. Field determination of soil hydraulic and chemical transport properties. Soil Sci. 167:353–368.

Arias-Estévez, M., E. López-Periago, E. Martínez-Carballo, J. Simal-Gándara, J.C. Mejuto, and L. García-Río. 2008. The mobility and degradation of pesticides in soils and the pollution of groundwater resources. Agric. Ecosyst. Environ. 123:247–260.

Bajracharya, K., and D.A. Barry. 1997. Nonequilibrium solute transport parameters and their physical significance: Numerical and experimental results. J. Contam. Hydrol. 24:185–204.

Bear, J., and Y. Bachmat. 1967. A generalized theory of hydrodynamics dispersion in porous media. p. 7–16. *In* Proc. IASH Symp.: Artificial Recharge and Management of Aquifers, Haifa. 19–26 Mar. 1967. Publ. 72. Int. Assoc. Hydrol. Sci., Paris.

Biggar, J.W., and D.R. Nielsen. 1976. Spatial variability of the leaching characteristic of a field soil. Water Resour. Res. 12:78–84.

Böhlke, J.K. 2002. Groundwater recharge and agricultural contamination. Hydrogeol. J. 10:153–179.

Butters, G.L., and W.A. Jury. 1989. Field scale transport of bromide in an unsaturated soil: 2. Dispersion modeling. Water Resour. Res. 25:1583–1598.

Casey, F.X.M., S.D. Logsdon, R. Horton, and D.B. Jaynes. 1998. Measurement of field soil hydraulic and solute transport parameters. Soil Sci. Soc. Am. J. 62:1172–1178.

Ghodrati, M., M. Chendorain, and Y.J. Chang. 1999. Characterization of macropore flow mechanisms in soil by means of a split macropore column. Soil Sci. Soc. Am. J. 63:1093–1101.

Hamilton, A.J., F. Stagnitti, X. Xiong, S.L. Kreidl, K.K. Benke, and P. Maher. 2007. Wastewater irrigation: The state of play. Vadose Zone J. 6:823–840.

Hanselman, T.A., D.A. Graetz, and A.C. Wilkie. 2003. Manure-borne estrogens as potential environmental contaminants: A review. Environ. Sci. Technol. 37:5471–5478.

Harter, T., and J.W. Hopmans. 2004. Role of vadose-zone flow processes in regional-scale hydrology: Review, opportunities, and challenges. p. 179–208. *In* R.A. Feddes et al (ed.) Int. Symp. on Unsaturated Zone Modelling: Progress, Challenges and Applications, Wageningen, the Netherlands. 3–5 Oct. 2004. Kluwer Acad. Publ., Dordrecht, the Netherlands.

Hills, R.G., P.J. Wierenga, D.B. Hudson, and M.R. Kirkland. 1991. The second Las Cruces Trench Experiment: Experimental results and two-dimensional flow predictions. Water Resour. Res. 27:2707–2718.

Hopmans, J.W., D.R. Nielsen, and K.L. Bristow. 2002. How useful are small-scale soil hydraulic property measurements for large-scale vadose zone modeling? p. 247–258. *In* P.A.C. Raats et al. (ed.) Environmental mechanics: Water, mass and energy transfer in the biosphere. Geophys. Monogr. 129. Am. Geophys. Union., Washington, DC.

Jaynes, D.B., and R.C. Rice. 1993. Transport of solutes as affected by irrigation methods. Soil Sci. Soc. Am. J. 57:1348–1353.

Jury, W.A. 1985. Spatial variability of soil physical parameters in solute migration: A critical literature review. EPRI EA-4228, Res. Proj. 2485-6. Elect. Power Res. Inst., Palo Alto, CA.

Jury, W.A., and H. Fluhler. 1992. Transport of chemicals through soil: Mechanisms, models and field applications. Adv. Agron. 47:142–201.

Jury, W.A., and K. Roth. 1990. Transfer functions and solute movement through

soil: Theory and applications. Birkhauser Verlag, Basel, Switzerland.
Jury, W.A., and G. Sposito. 1985. Field calibration and validation of solute transport for the unsaturated zone. Soil Sci. Soc. Am. J. 49:1331–1341.
Jury, W.A., L.A. Stolzy, and P. Shouse. 1982. A field test of the transfer function model for predicting solute transport. Water Resour. Res. 18:369–375.
Kachanoski, R.G., E. Pringle, and A. Ward. 1992. Field measurement of solute travel times using time domain reflectometry. Soil Sci. Soc. Am. J. 56:47–52.
Kellogg, R.L., C.H. Lander, D.C. Moffitt, and N. Gollehon. 2000. Manure nutrients relative to the capacity of cropland and pastureland to assimilate nutrients: Spatial and temporal trends for the United States. GSA Publ. nps00-0579. Gen. Serv. Admin., Fort Worth, TX.
Li, Y., and M. Ghodrati. 1997. Preferential transport of solute through soil columns containing constructed macropores. Soil Sci. Soc. Am. J. 61:1308–1317.
Mass, E.V., and G.J. Hoffman. 1977. Crop salt tolerance: Current assessment. J. Irrig. Drain. Div. Am. Soc. Civ. Eng. 103:115–134.
Peterson, E.W., R.K. Davis, and H.A. Orndorff. 2000. 17 β-Estradiol as an indicator of animal waste contamination in mantled karst aquifers. J. Environ. Qual. 29:826–834.
Poulsen, T.G., P. Moldrup, L.W. de Jonge, and T. Komatsu. 2006. Colloid and bromide transport in undisturbed soil columns: Application of two-region model. Vadose Zone J. 5:649–656.
Richards, L.A. 1931. Capillary conduction of liquids in porous mediums. Physics 1:318–333.
Roth, K., W.A. Jury, H. Fluhler, and W. Attinger. 1991. Transport of chloride through an unsaturated field soil. Water Resour. Res. 27:2533–2541.
Segal, E., S.A. Bradford, P. Shouse, N. Lazarovitch, and D. Corwin. 2008. Integration of hard and soft data to characterize field-scale hydraulic properties for flow and transport studies. Vadose Zone J. 7:878–889.
Šimůnek, J., K. Huang, M. Šejna, and M.Th. van Genuchten. 1999. The HYDRUS-2D software package for simulating two-dimensional movement of water, heat and multiple solutes in variably-saturated media. Version 2.0. IGWMC-TPS-53. Int. Ground Water Model. Ctr., Colorado School of Mines, Golden.
Šimůnek, J., M. Sejna, and M.T. van Genuchten. 1998. The HYDRUS-1D software package for simulating the one-dimensional movement of water, heat, and multiple solutes in variably saturated media. Version 2.0. U.S. Salinity Lab., Riverside, CA.
Thomasson, M.J., P.J. Wierenga, and T.P.A. Ferre. 2006. A field application of the scaled-predictive method for unsaturated soil. Vadose Zone J. 5:1093–1110.
Vanderborght, J., A. Timmerman, and J. Feyen. 2000. Solute transport for steady-state and transient flow in soils with and without macropores. Soil Sci. Soc. Am. J. 64:1305–1317.
Vanderborght, J., and H. Vereecken. 2007. Review of dispersivities for transport modeling in soils. Vadose Zone J. 6:29–52.
van Genuchten, M.Th. 1980. A closed-form equation for predicting the hydraulic conductivity of unsaturated soils. Soil Sci. Soc. Am. J. 44:892–898.
van Genuchten, M.Th., and P.J. Shouse. 1989. Solute transport in heterogenous field soils. p. 177–187. *In* D.T. Allen et al. (ed.) Intermedia pollutant transport. Plenum Publ., New York.
van Genuchten, M.Th., and P.J. Wierenga. 1977. Mass transfer studies in sorbing porous media: I. Analytical solutions. Soil Sci. Soc. Am. J. 40:473–480.
Vereecken, H., R. Kasteel, J. Vanderborght, and T. Harter. 2007. Upscaling hydraulic properties and soil water flow processes in heterogeneous soils: A review. Vadose Zone J. 6:1–28.
Vogeler, I., S. Green, A. Nadler, and C. Duwig. 2001. Measuring transient solute transport through the vadoze zone using time domain reflectometry. Aust. J. Soil Res. 39:1359–1369.
Wani, P.A., M.S. Khan, and A. Zaidi. 2007. Impact of heavy metal toxicity on plant growth, symbiosis, seed yield and nitrogen and metal uptake in chickpea. Aust. J. Exp. Agric. 47:712–720.
Ward, A.L., R.G. Kachanoski, and D.E. Elrick. 1994. Laboratory measurements of solute transport using time domain reflectometry. Soil Sci. Soc. Am. J. 58:1031–1039.
Watson, K.K. 1966. An instantaneous profile method for determining the hydraulic conductivity of unsaturated porous materials. Water Resour. Res. 2:709–715.
Wierenga, P.J., and M.Th. van Genuchten. 1989. Solute transport through small and large unsaturated soil columns. Ground Water 27:35–42.
Zhang, Z.F., A.L. Ward, and G.W. Gee. 2003. Estimating soil hydraulic parameters of a field drainage experiment using inverse techniques. Vadose Zone J. 2:201–211.
Zhu, J., and B.P. Mohanty. 2002. Spatial averaging of van Genuchten hydraulic parameters for steady-state flow in heterogeneous soils: A numerical study. Vadose Zone J. 1:261–272.
Zurmuhl, T. 1998. Capability of convection–dispersion transport models to predict transient water and solute movement in undisturbed soil columns. J. Contam. Hydrol. 30:101–128.